Volume 10
Number 9
September 2023
Pages 3177–3856

# Materials Horizons

rsc.li/materials-horizons

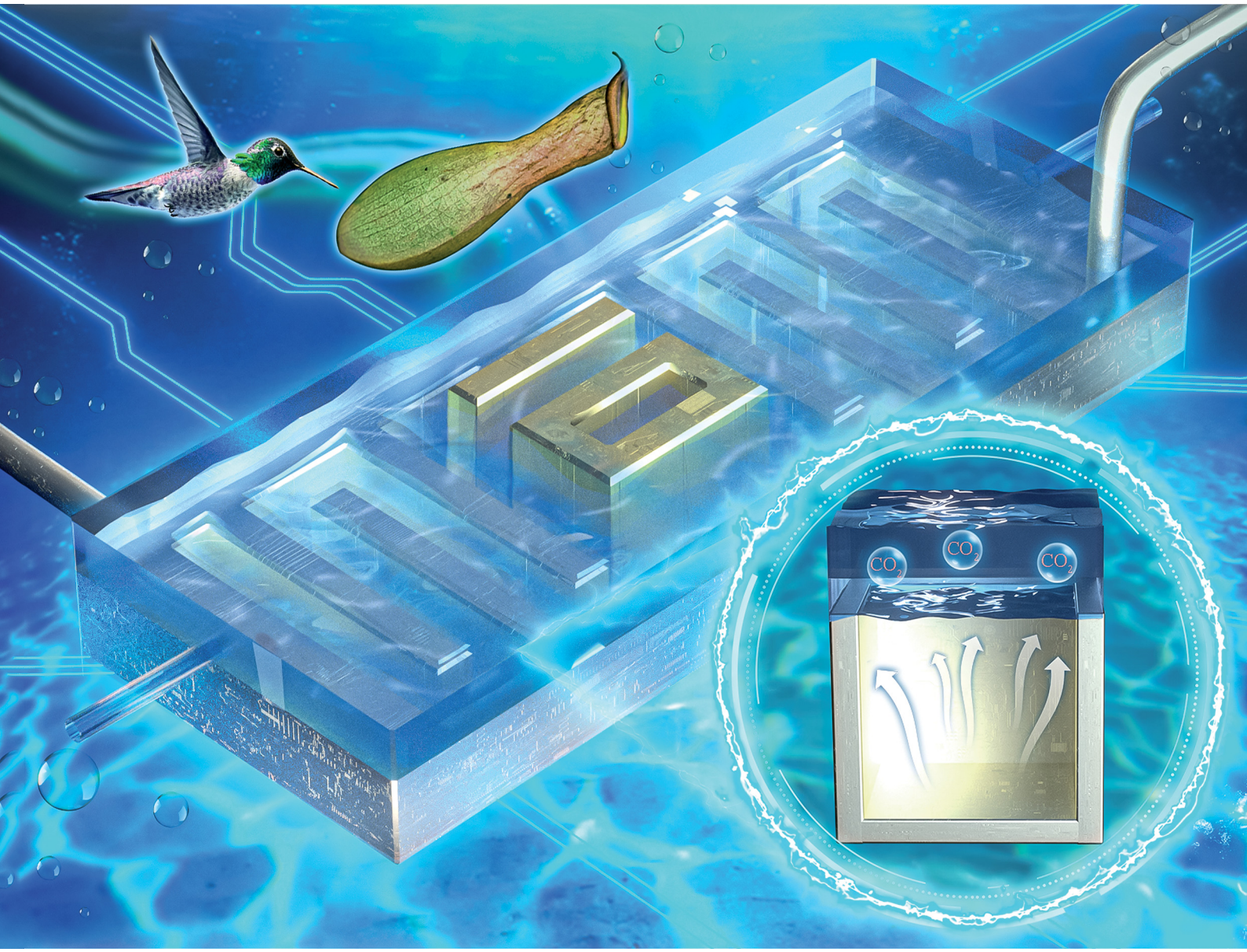


ISSN 2051-6347

ROYAL SOCIETY OF CHEMISTRY

**COMMUNICATION**

Moyuan Cao *et al.*

Designing a slippery/superaerophobic hierarchical open channel for reliable and versatile underwater gas delivery

Materials Horizons

ROYAL SOCIETY OF CHEMISTRY

COMMUNICATION

View Article Online
View Journal | View Issue

Check for updates

Cite this: *Mater. Horiz.*, 2023, **10**, 3351

Received 12th June 2023,
Accepted 10th July 2023

DOI: 10.1039/d3mh00898c

rsc.li/materials-horizons

Published on 11 2023. Downloaded on 2024/10/12 2:17:48.

# Designing a slippery/superaerophobic hierarchical open channel for reliable and versatile underwater gas delivery†

Xinsheng Wang,[a] Haoyu Bai,[ac] Zhe Li,[ac] Yaru Tian,[a] Tianhong Zhao[a] and Moyuan Cao *[ab]

**Achieving long-term and stable gas manipulation in an aqueous environment is necessary to improve multiphase systems relating to gas/liquid interaction. Inspired by the Pitcher plant and the hummingbird beak, we report a slippery/superaerophobic (SLSO) hierarchical fluid channel for continuous, durable, and flexible gas transport. The immiscible lubricant layer inside the SLSO channel promotes one-year stability of gas transport, and the maximum flux of this open channel can reach 3000 mL $h^{-1}$. Further integration of a $CO_2$ capturing microchip demonstrates the availability and potential of this gas-manipulating interface, which should provide a valuable platform to develop advanced materials and devices.**

[a] *School of Materials Science and Engineering, Smart Sensing Interdisciplinary Science Centre, Nankai University, Tianjin 300350, P. R. China. E-mail: mycao@nankai.edu.cn, moyuan.cao@tju.edu.cn*

[b] *Haihe Laboratory of Sustainable Chemical Transformations, Tianjin 300192, P. R. China*

[c] *School of Chemical Engineering and Technology, Tianjin University, Tianjin, 300072, P. R. China*

† Electronic supplementary information (ESI) available. See DOI: https://doi.org/10.1039/d3mh00898c

**Moyuan Cao**

*Materials Horizons has formed an excellent reputation over the last ten years. As the flagship journal of the RSC in materials science, many excellent studies have been published within the fields of polymer science, materials chemistry, energy device, bioinspired materials, etc. The innovation of this work is the decisive factor in publishing in Materials Horizons, making this journal positive and unbiased. I'm honored to be an advisory board member and to have won the outstanding paper runner-up prize in 2018. Happy 10th anniversary to Materials Horizons.*

## New concepts

In nature, aquatic animals have evolved a lot of unique structures to obtain oxygen for their better survival. Inspired by the natural open surfaces possessing a gas manipulating ability, scientists have invented a series of advanced interfacial materials for the enhancement of gas/liquid exchange and gas-involved chemical reactions. For the commonly used superaerophilic surface, its long-term gas transport would be gradually deteriorated due to the loss of gas films. In comparison, a lubricant-infused slippery surface with an immiscible and uncompressible liquid layer would provide a more stable platform to control gas behavior in an aqueous environment. By taking bioinspiration from the Pitcher plant and the humming bird's beak, here we propose a continuous and reliable gas-transporting channel with a hierarchical structure and open surface for versatile gas manipulation. This channel can maintain its gas-transporting ability after one-year of water soaking, which is largely improved as compared with a superhydrophobic channel. Our design will offer more options to develop gas/liquid related advanced devices in the fields of aeration, $CO_2$ capture, catalysis, *etc.*

Optimizing the interfacial interaction from the nanoscale to macroscale is essential to improve the performance of current systems such as heterogeneous catalysis,[1,2] gas absorption,[3,4] biomedical materials,[5,6] *etc.* The rational control of the fluid behaviour on the functional interfaces is the key to boosting the interfacial reaction and mass transfer. For example, Feng's group reported a series of superaerophilic carriers for increasing the efficiency of both enzyme sensors[7] and photocatalysis,[8] and the continuous and spontaneous gas supply can maintain the local oxygen concentration and device performance. The continuous pumping of liquid onto a solar evaporating surface *via* well-defined superhydrophilic substrates is capable of enlarging the evaporation area and then accelerating the evaporation rate.[9,10] A porous fabric with Janus wettability is able to transport liquid unidirectionally, which is suitable for the wound dressings and smart clothes for biofluid outward delivery.[11–13]

Thanks to natural selection, animals and plants have evolved versatile methods to manipulate fluid for feeding, cooling, attack, *etc.* Therefore, inspiration from nature should

Published on 11 2023. Downloaded on 2024/10/12 2:17:48.

give us inexhaustible ideas for designing advanced interfaces that possess spontaneous, continuous, smart, and integrable fluid transporting abilities.[14–16] The natural strategy of controlling on-surface fluid transport mainly depends on asymmetric factors such as wettability difference,[17,18] oriented microstructures,[19,20] and geometric gradients,[21,22] for example, butterfly proboscis exhibiting a hydrophobic outer surface and a hydrophilic inner tube, which can guarantee liquid feeding without leakage.[23] By using hydrophilic oriented scales, the Texas horn lizard (*Phrynosoma cornutum*) can achieve spontaneous water uptake with a relatively static posture.[24] Through the fusion of a ratchet structure and a conical channel, the shorebird can drink easily *via* the reciprocally open/close motion of the long beak.[25] To survive in water for a long time, the diving bell spider (*Argyroneta aquatica*) is able to transport air bubbles into water *via* its superhydrophobic furry back.[26] As a consequence, the bioinspired fluid transport is preferentially based on an open channel and an asymmetric structure, which should be a better way to enhance the mass/energy transfer and control the fluid behaviour.[27–29]

Compared with liquid manipulation, it is also valuable to investigate underwater gas control due to the potential applications in aeration,[30] gas-involved catalysis,[31] water splitting,[32] anticounterfeiting,[33] *etc.* Superhydrophobic substrates, *i.e.*, commonly known as underwater superaerophilic substrates, have emerged as a powerful platform to realize highly-efficient gas/liquid exchanging processes.[34–36] The considerable gas transporting capacity on superaerophilic surfaces promotes a reliable method to control the gas accumulation, transfer and distribution toward specific application scenarios.[37] However, the current method based on a superhydrophobic system is not durable enough to achieve long-term underwater availability. For most situations, the gas film on the submerged superhydrophobic surface may be gradually deteriorated in a few days, originating from the inevitable dissolving of the gas film.[38,39] Although the incorporation of an external gas source can improve the stability of a superaerophilic surface, the complicated design may influence the conformability and flexibility of such interfaces.

A slippery surface with an uncompressible lubricant layer shows improved stability under a harsh environment.[40–42] In an aqueous environment, the water-immiscible lubricant layer also exhibits aerophilic properties, promoting a durable, flexible and functional bubble manipulating process.[43] Owing to the insufficient gas capturing ability, the continuous gas flow transport on this slippery surface is still a challenge. By taking inspiration from the Pitcher plant and the hummingbird beak, here we report a slippery/superaerophobic (SLSO) hierarchical open channel for reliable, continuous, and functional gas manipulation under water. The SLSO channel is composed of an aerophilic slippery groove for gas transport and a superaerophilic edge for retaining gas. On the basis of the hierarchical structure of the open gas channel, the maximum capacity of the single SLSO channel can reach 3000 mL $h^{-1}$ which is three times higher than that of the slippery channel without hierarchical wettability. More importantly, the durability of this SLSO channel is largely improved, *i.e.*, the gas transporting ability can be maintained after one-year of water soaking. Taking advantage of the 3D printing technique, the SLSO channels with various features such as U-shape, Y-shape, wave-shape, spiral and assembled structures can be facilely designed for versatile gas manipulation. In addition, the gas/liquid exchanging microchip with continuous SLSO folded channels was proposed for on-chip $CO_2$ absorption. We envision that this durable gas transporting channel should offer us great opportunities to improve the underwater gas-related interface, and update our knowledge of bioinspired fluid controlling systems with long-term stability.

The development of a lubricant-infused surface inspired by pitcher plants has demonstrated its effectiveness in manipulating underwater gas.[44,45] This surface has outperformed superhydrophobic air carriers, by showing greater stability and durability in its gas manipulating capacity. To further enhance this ability, a hierarchical structure has been designed to control a high-flux and continuous gas flow within a bioinspired SLSO channel (Fig. 1(a)). Our approach has drawn inspiration from the dynamic fluid trapping structure observed in the hummingbird beak, which is capable of stably locking water within the channel.[46,47] By combining the structural features of the hummingbird' beak with lubricant-infused surfaces, we have successfully created a stable open channel for transporting gas in underwater applications. The SLSO hierarchical gas channel exhibits a distinctive and layered architecture, characterized by a hydrophobic lubricant-infused surface and a superaerophobic surface. The inner surface of the channel is found to be aerophilic, exhibiting a bubble contact angle of $84.7^\circ \pm 2.8^\circ$ (Fig. 1(b)) and the water contact angle is $95.2^\circ \pm 1.1^\circ$. In contrast, the upper surface of the channel is superaerophobic, displaying a bubble contact angle of $147.2^\circ \pm 4.9^\circ$ (Fig. 1(b)) and the water contact angle is $5.9^\circ \pm 1.5^\circ$. The gas flow in the channel is found to be stable due to the synergistic interplay between the gas adsorption by the aerophilic inner surface and the gas confinement by the superaerophobic upper surface (Fig. 1(c) and Movies S1, S2, ESI†).

To enable the production of complex structured devices, the use of a 3D printable polylactide (PLA) material has been selected for constructing the slippery/superhydrophobic (SLSO) hierarchical gas channels. The procedure for fabricating these channels is depicted in Fig. 1(b). Initially, the PLA channels are generated through 3D printing technology. Subsequently, a light-curing coating, comprising of vinyl triethoxy silane (VTES), hydrophobic complementary silica (HFS), and photoinitiator (Darocure 1173), is utilized to establish a superhydrophobic porous structure (Fig. S1, ESI†) on the internal surface of the 3D printed channel. A superhydrophilic coating, containing a silica sol and a hydrophilic cellulose-based polymer, is then applied on the upper surface of the channel. Finally, to achieve a stable lubricant-infused surface, dimethyl silicone oil ($\sim$50 mPa S) is deposited onto the superhydrophobic surface on the inner side of the channel. As shown in the SEM images (Fig. S1e and f, ESI†) and

 This journal is © The Royal Society of Chemistry 2023

Published on 11 2023. Downloaded on 2024/10/12 2:17:48.

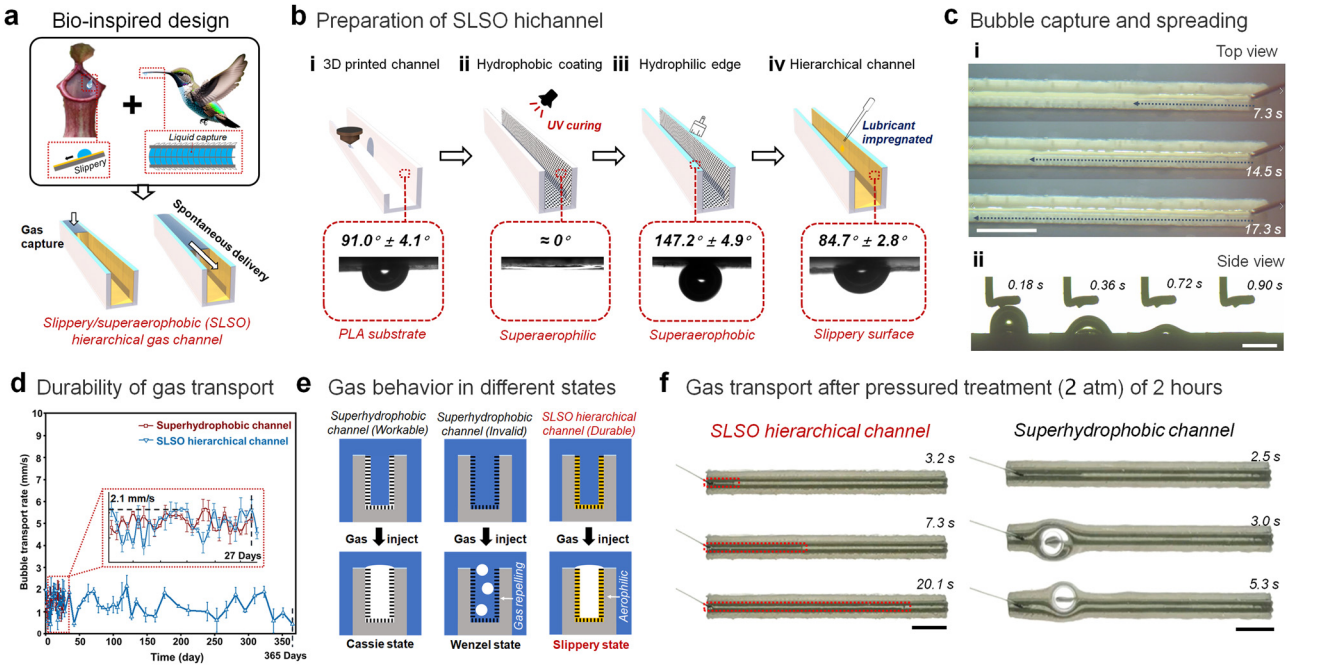


Fig. 1 Design and preparation of the SLSO hierarchical gas channel. (a) Bio-inspiration of the SLSO hierarchical gas channel-combination from the slippery surface of the Pitcher plant and the water-locking structure of the hummingbird beak. (b) The fabrication process of the SLSO hierarchical gas channel based on 3D printing technology, the insets represent the contact angles of underwater bubbles on the surface in the corresponding steps, respectively. (c) The gas spreading process in the SLSO hierarchical gas channel, the top view of the gas injection process (i) with a scale bar of 1 cm, and side view of the spreading process of the 4ul bubble, scale bar 2 mm. (d) The durability test of the superhydrophobic channel and SLSO hierarchical channel immersed in water was performed by pumping gas into the channels at a rate of 10 ml per hour per day. The superhydrophobic channel becomes invalid after 27 days, while the SLSO hierarchical channel was still able to transport gas after 365 days. (e) The mechanism of the difference in durability between the superhydrophobic channel and the SLSO hierarchical channel is that the gas film in the superhydrophobic channel is prone to failure, resulting in the gas channel clogging. In contrast, the lubricant layer in the SLSO hierarchical channel is uncompressible and stable. (f) Comparison of gas transport processes during the SLSO hierarchical channel and superhydrophobic channel after a pressure treatment of 2 atm for two hours, scale bar 1 cm.

microscope images (Fig. S2, ESI†), the hydrophilic coating on the upper surface and the hydrophobic porous coating on the inner surface are clearly demarcated at the corners. The thickness of the hydrophilic coating is about 20 μm, and the hydrophilic post-treatment does not affect the hydrophobic porous structure inside the channel.

The use of a SLSO hierarchical channel for underwater gas manipulation has been investigated, and it has been demonstrated that it offers higher durability compared to a standard superhydrophobic channel. This can be primarily attributed to the incompressibility and fluidity of the lubricant present within the SLSO hierarchical channel. Immersion experiments conducted for a duration of 27 days suggest that the superhydrophobic gas channel becomes ineffective, whereas the SLSO hierarchical gas channel remains effective even after 365 days (Fig. 1(d), Fig. S3 and Movie S3, ESI†). Additionally, the SLSO hierarchical gas channel exhibits superior pressure resistance (Movie S4, ESI†), as indicated by the stable gas transport accomplished after 2 hours of exposure to high-pressure (2 atm) and low-pressure (20 kPa) conditions (Fig. 1(f)). In contrast, the superhydrophobic channel failed under similar conditions (Fig. S4, ESI†). The gas film on the micro-/nano-structure of the superhydrophobic surface is the key to capturing the gas in an aqueous environment. When the superhydrophobic surface is wetted, the gas film will be replaced by water, resulting in a gas repellent surface. Even if being continuously charged onto the surface, it is difficult for the gas with a low density to displace the water away from the wetted superhydrophobic surface. Therefore, the superhydrophobic channel will lose the ability to manipulate gas. The superior performance of the SLSO hierarchical gas channel can be attributed to the stability and incompressible properties of its lubricant, which enables significant durability even under extreme pressure conditions or immersion. On the other hand, the gradual replacement of the gas film by water due to immersion or pressure treatment causes the transition from the Cassie state to the Wenzel state of the superhydrophobic surface, leading to its ineffectiveness.

The key component of the SLSO hierarchical gas channel, which allows for low resistance gas transport, is the aerophilic lubricant-infused surface. Gas can stably spread in a 1 mm wide aerophilic lubricant-infused channel. The gas column acquires a forward-spreading curved structure, which is directly attributed to the presence of aerophilic surfaces on both sides of the channel. The curved structure generates a Laplace pressure that facilitates the efficient spreading of gas bubbles within the

Published on 11 2023. Downloaded on 2024/10/12 2:17:48.

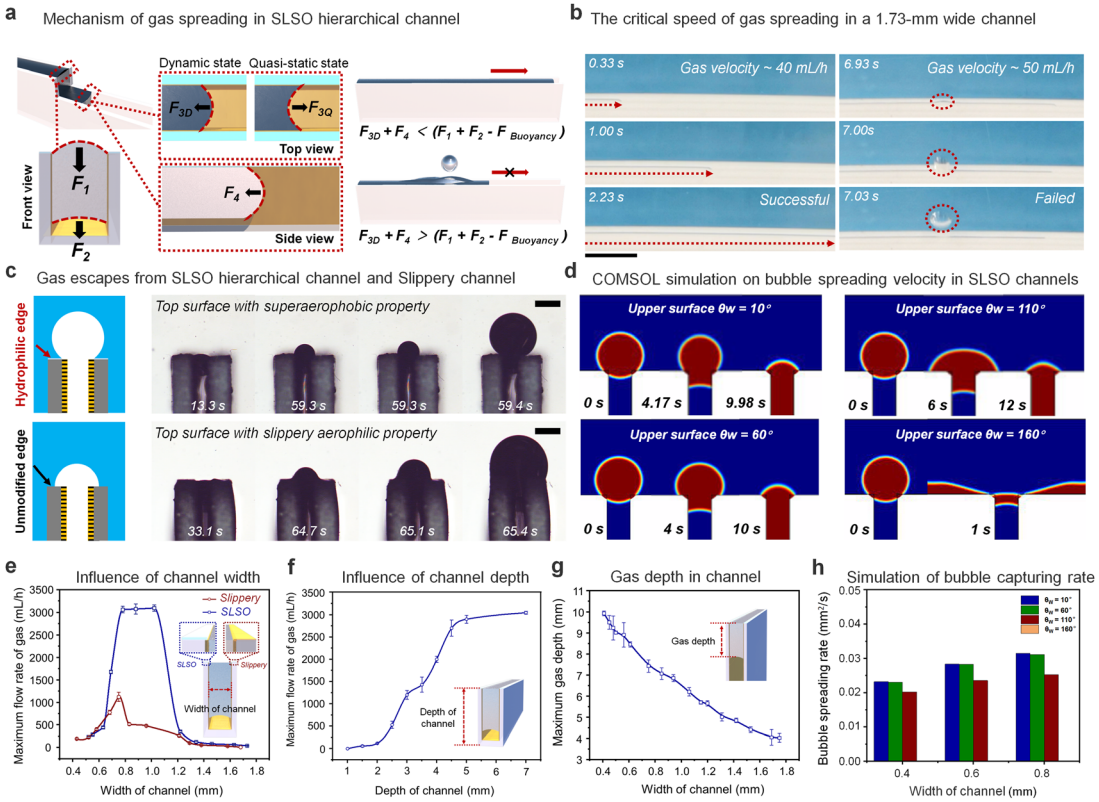


Fig. 2 Gas transport in the SLSO hierarchical gas channel. (a) Mechanistic analysis of the spreading process of gas in the channel, including the spreading process of gas in the channel and the process of escape on the upper surface. (b) The gas transport process in a 1.73 mm wide SLSO hierarchical channel at below and above the critical gas speed, scale bar = 1 cm. (c) The escape process of gas in the channel. When the edge surface is superhydrophilic, the lubricant does not spread on the upper surface. In comparison, when the upper surface is unmodified, the lubricant tends to spread on the edge surface, resulting in an aerophilic edge. Scale bar = 1 mm. (d) COMSOL multiphysics simulation of the front view of the bubble spreading in the SLSO hierarchical gas channel. The water contact angles on the upper surface are 10°, 60°, 110° and 160° respectively. (e) As the width of the channel increases, the critical rate of gas injection tends to increase and then decrease. Moreover, whether the upper surface is superhydrophilic has an obvious effect. (f) With the increase of channel depth, the limiting rate of gas injection shows a trend of increasing and then remaining constant, which is related to the depth of dynamic spreading of gas in the channel. (g) At the quasi-static state, the spread depth of the gas in the channel is inversely proportional to the channel width. (h) The spreading speed of a bubble spread into the channels with different upper surface water contact angles, which was obtained by COMSOL Multiphysics simulation. The result indicates the larger the water contact angle of the edge surface, the slower the bubble spreading.

channel, as depicted in Fig. 2(a) for $F_1$, $F_2$, and $F_{3Q}$. The Laplace pressure ($P_L$) can be mathematically described by eqn (1):[48]

$$P_L = \gamma_{water}\left(\frac{1}{R_1} + \frac{1}{R_2}\right) \quad (1)$$

where $R_1$ and $R_2$ are the radius of curvature in the transverse and longitudinal directions, respectively, and $\gamma_{water}$ is the surface tension of the air/water interface. For $F_1$ and $F_2$, the transverse radius of curvature is shown in the front view of Fig. 2(a), while the longitudinal radius of curvature can be regarded as infinite because the gas is infinitely spread forward in the channel. Therefore, as curvature and radius decrease, Laplace pressure increases accordingly.

As the gas spreads forward, a drag force is formed on both surfaces due to the presence of contact angle hysteresis,[49] as shown in the following equation.

$$F_R = \frac{1}{2}C_D\rho v^2 S + av^k + F_{CAH} \quad (2)$$

where $C_D$ is the drag coefficient of water, $\rho$ is the density of water, $v$ is the bubble velocity, and $S$ is the contact area between the gas and the inner surface of the channel. $a$ and $k$ are the undefined parameters for the resistance force from the potential deformation of the lubricant layer. $F_{CAH}$ is the resistance of contact angle hysteresis that can be estimated by eqn (3).

$$F_{CAH} = 2w\gamma_{water}\cdot(\cos\theta_r - \cos\theta_a) \quad (3)$$

where $w$ is the gas spreading depth in the channel, and $\theta_r$ and $\theta_a$ are the receding and the advancing angles on the corresponding surface, respectively.

When the gas spreads forward at a high rate, the top view reveals a convex forward curvature of the gas column. This curvature gives rise to a Laplace pressure that acts in a backward direction and thereby hinders the forward transport of the gas. This phenomenon is exemplified in Fig. 2(a) for $F_{3D}$. Experimental findings show that the gas spreading forward within the channel induces an outwardly convex curvature in

 This journal is © The Royal Society of Chemistry 2023

Published on 11 2023. Downloaded on 2024/10/12 2:17:48.

the vertical direction, which itself generates an inward Laplace pressure.

In the presence of resistance, gases tend to move in the direction of least resistance. Accordingly, when the resistance towards horizontal movement is less than the resistance required to exit the upper surface ($F_{3D} < F_1 + F_2 - F_{Buoyancy}$), the gas will spread out horizontally. As the gas spreading velocity increases, the resistance towards horizontal movement gradually increases. When the resistance towards horizontal movement becomes greater than the resistance needed to exit above the channel ($F_{3D} > F_1 + F_2 - F_{Buoyancy}$), the gas will escape through the upper surface of the channel instead of spreading within it. Fig. 2(b) and Movie S5 (ESI†) provide insight into gas injection velocity during critical velocity attainment and over-attainment. Without critical velocity attainment, gas fills up the entire channel. However, upon exceeding the critical velocity threshold, the gas escapes through the upper side of the channel.

An investigation into the impact of a superhydrophilic layer on the upper surface of a channel on the gas escape process has been conducted (Fig. 2(c) and Movie S6, ESI†). When the edge surface is modified with a superaerophobic layer, the lubricant fails to remain on the upper surface due to the intrusion of hydrophilic coating (Fig. S5 and Movie S7, ESI†). Due to the large bubble contact angle ($147.2^\circ \pm 4.9^\circ$) associated with the superhydrophilic surface, the extruded bubble displays a higher curvature and Laplace pressure during the escape process. Conversely, when the upper surface is not treated with superhydrophilic coating, the lubricant adheres to the upper surface. The lack of a superhydrophilic layer on the upper surface causes the gas to spread on this surface. This results in the inability of the gas to form a larger curvature and increased susceptibility to escape upwards with less resistance. The application of a superficial surface superhydrophilic treatment restricts the spreading of bubbles in the channel, as illustrated through the analysis of the limiting transport velocity of gas in the channel (Fig. 2(e)). The channel treated with superhydrophilic coating on the upper surface demonstrates a higher ultimate gas injection velocity of 3000 mL $h^{-1}$ compared to 1200 mL $h^{-1}$ for the channel without hydrophilic treatment on the upper surface. These results demonstrate the stability and advantages of the SLSO hierarchical channel in gas transport. Additionally, as the channel depth decreases, the limiting transport velocity of the bubble also decreases (Fig. 2(f)), primarily due to the curvature of the gas during spreading (Fig. S6, ESI†). The curvature of the advancing direction of the gas column increases with the decrease in gas column thickness, resulting in an increase in spreading resistance.

To further investigate the influence of the wettability of the upper surface of the channel on the adsorption process of bubbles, we conducted COMSOL Multiphysics simulations, as presented in Fig. 2(d). The simulation analysed the effect of the upper surface's wettability on the adsorption of bubbles (radius = 0.4 mm). The results showed that when the upper surface demonstrated hydrophilic characteristics (upper surface $\theta_w$ = $10^\circ$ or $60^\circ$), the bubble adsorption occurred quickly. On the other hand, when the upper surface demonstrated ordinary hydrophobic behaviour (upper surface $\theta_w = 110^\circ$), the bubble entered the channel with lateral deformation behaviour and a slower adsorption rate. Furthermore, the simulation indicated that a superhydrophobic upper surface (upper surface $\theta_w$ = $160^\circ$) resulted in a preference for the bubble to spread on the upper surface rather than in the channel. Additionally, Fig. 2(h) illustrates the bubble spreading velocity for channels of different widths. The adsorption velocity of the bubbles gradually decreased as the aerophilicity of the upper surface increased.

The relationship between the channel width and the spreading depth of gas within the channel was further investigated. Through our investigation, it was observed that there existed a negative correlation between the channel width and the spreading depth of the gas within the channel, as illustrated in Fig. 2(g). This process was quasi-static, and force analysis was conducted to delineate the underlying mechanism.

$$F_{Buoyancy} = F_1 + F_2 \quad (4)$$

where the buoyancy force can be calculated from eqn (5).

$$F_{Buoyancy} = \rho g V_{Bubble} = \rho g D L H \quad (5)$$

where $\rho$ is the density of water, $D$ is the width of the gas channel, $L$ is the spreading length of the gas in the channel, $g$ is the gravitational acceleration, and $H$ is the spreading depth of the gas in the channel.

$F_1$ and $F_2$ can both be expressed by the capillary force formula (eqn (6)).

$$F_1 + F_2 = \gamma_{water}(\cos\theta_u - \cos\theta_l)2L \quad (6)$$

where $\theta_u$ and $\theta_l$ are the contact angles between the upper side of the air column to the channel and the lower side to the channel, respectively. Thus, the relationship between the spread depth ($H$) of the gas in the channel and the channel width ($D$) can be analyzed with eqn (7).

$$D \times H = \frac{2\gamma(\cos\ \theta_u + \cos\ \theta_l)}{\rho g} \quad (7)$$

Specifically, the force analysis showed that the effective force exerted on the gas in the channel was a result of the pressure drop across the channel, as determined by the channel geometry and gas flow rate. Hence, a larger channel width correspond to a smaller pressure drop, leading to a reduced effective force and, consequently, a shallower spreading depth of the gas within the channel.

The force analysis in Fig. 2 proves that the spreading process of the gas in the channel is independent of the channel length, so theoretically, by considering the maximum Laplace pressure resulted from the single curved surface perpendicular to the channel ($P_L = 2\gamma_{water}/D$), the gas column can be stably trapped in the channel, promoting an infinite spreading in the channel. In addition, the spiral channel and the wave channel in Fig. 3 can partly prove that the gas can spread for a long distance in the channel.

Published on 11 2023. Downloaded on 2024/10/12 2:17:48.

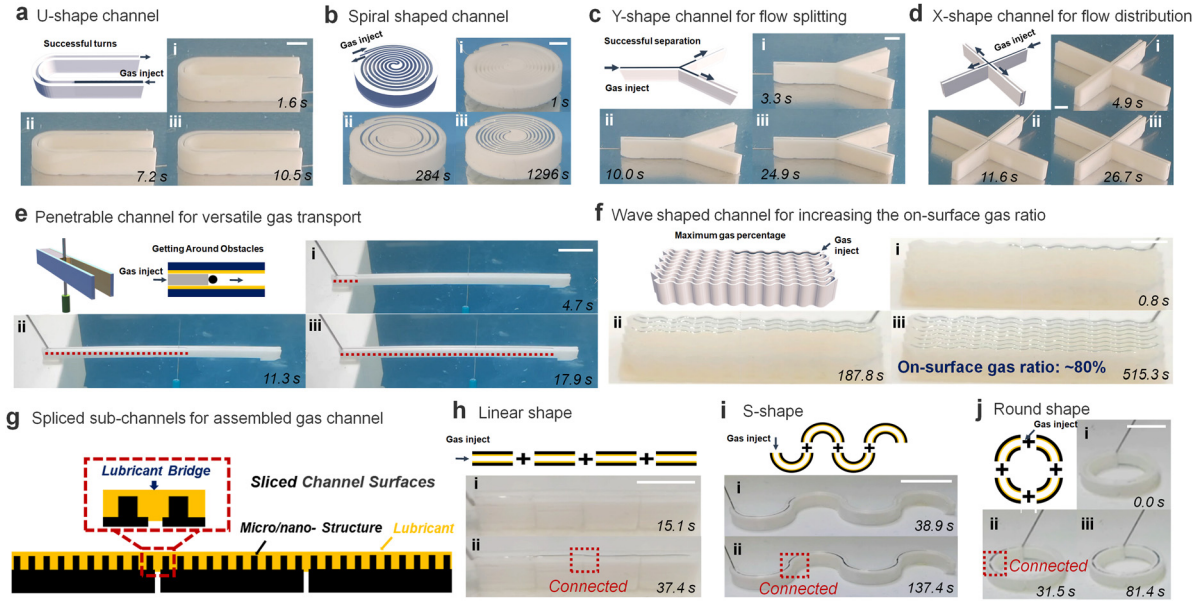


Fig. 3 On-demand gas transport in versatile SLSO hierarchical gas channels. Gas transport process in the (a) U-shape, (b) spiral, (c) Y-shape, and (d) X-shape SLSO hierarchical gas channel. (e) Gas transport process in the penetrable hollow SLSO hierarchical gas channel. Gas flow can easily pass through the barrier of a steel needle. (f) The gas transport process in the folded wavy SLSO hierarchical gas channel, and the final on-surface gas ratio can reach 80%. (g) Schematic diagram of the assembly of the spliced SLSO hierarchical gas channels. The lubricant can spontaneously form a liquid bridge over the splice, resulting in a continuous slippery channel for gas transport. The assembled SLSO channels with (h) linear, (i) S-shape, and (j) O-shape.

In addition, the SLSO hierarchical gas channel can achieve gas transport under many complicated conditions, which provides the foundation for the practical application of the SLSO hierarchical gas channel. Notably, our observations indicated that even when the channel is subjected to sharp curvature. Such as in the U-shaped configuration shown in Fig. 3(a), the gas is able to effectively occupy the entire channel without being significantly affected by column deformation. (Movie S8, ESI†). This was further demonstrated in the double-spiral channel design as depicted in Fig. 3(b), which exhibited no evidence of gas leakage despite the presence of spiral structures along the channel. Not only in the curved channel, but also in the bifurcated channel. As in the Y-shape gas channel (Fig. 3(c)) and the X-shape gas channel (Fig. 3(d)), the gas can overcome the deformation at the bifurcation and fill the whole channel (Movie S8, ESI†). Various examples have shown the stability of the SLSO hierarchical gas channel in transporting gas underwater.

Another advantage of the SLSO hierarchical gas channel is its ability to greatly increase the gas–liquid contact area by utilizing a penetrable hollow channel design, as depicted in Fig. 3(e) and Movie S9 (ESI†). This hollow SLSO channel design possesses double the gas–liquid interface area compared to the aforementioned solid SLSO hierarchical channel, as a result of the capillary force tightly holding the gas–liquid interface along the channel wall. In addition, the gas can bypass the needle-like obstacle when transporting forward in the channel, which further illustrates the stability of gas transport in the channel. The gas–liquid contact area can also be enhanced by reducing the wall thickness of the gas channels. In the case of a straight-walled channel design, the stability of the channel is only maintained for wall thicknesses exceeding 0.8 mm, resulting in a limited surface gas area of 50%. To overcome this limitation, the SLSO hierarchical gas channel has been redesigned into a wave-shaped geometry. As shown in Fig. 3(f) and Movie S10 (ESI†), a wave-shaped channel with a wall thickness of 0.2 mm and a width of 0.8 mm is designed, and the area occupied by the gas is 80%. Specifically, when the channel is straight, it can easily deform due to the liquid capillary self-assembly[50] which limits its applicability. However, the wave-shaped design, with the same wall thickness as the straight channel, enhances the mechanical strength of the channel, thereby eliminating the influence of capillary effects and resulting in a higher on-surface gas ratio for the SLSO channel.

Previous studies have demonstrated that the splicing of lubricant-infused surfaces does not impede the movement of gas bubbles at the spliced region.[51] This is due to the self-healing capabilities of lubricant-infused surfaces. Specifically, when two independent lubricant-infused surfaces are assembled tightly, lubricant spontaneously generates a liquid bridge, resulting in a continuous, well-distributed layer for the lubrication of the entire channel (Fig. 3(g)). This principle can also be applied to the SLSO hierarchical gas channel. When multiple spliced SLSO hierarchical gas channels are assembled, the self-healing property of the lubricant-infused inner surface facilitates the smooth passage of gas through the channel splice. It is worth emphasizing that this self-healing behaviour is essential for minimizing the adverse effects associated with gas flow interruptions at the spliced channel regions. Therefore, the lubricant-infused design of the SLSO hierarchical gas channel offers a viable solution for the splicing of multiple channels

 This journal is © The Royal Society of Chemistry 2023

Published on 11 2023. Downloaded on 2024/10/12 2:17:48.

without compromising their overall performance. As shown in Fig. 3(h), the gas can be transported smoothly in the linear spliced SLSO hierarchical gas channel. Notably, the spliced design of the SLSO hierarchical gas channel permits more than just linear configurations (Fig. 3(h)). As depicted in Fig. 3(i) and (j), both S-shaped and O-shaped spliced SLSO hierarchical gas channels exhibit the potential for complete gas transport (Movie S11, ESI†). Accordingly, the SLSO hierarchical gas channel can be assembled by splicing to achieve more complex underwater gas transport processes, which increase the practical application capability of the SLSO hierarchical gas channel.

The current technologies of $CO_2$ capture mainly include chemical sorbents, physical absorption, and membrane process. The $CO_2$ capture mechanisms of these methods are different, which depends mainly on the physical and chemical properties of the materials employed. For example, in the monoethanolamine (MEA) absorbing method that we used, carbon dioxide is based on its interaction with the amine to form a hydrocarbon salt or carbamate, resulting in a relatively mild condition and low-cost equipment. Liquid sorbent is a method of $CO_2$ enrichment by absorbing $CO_2$ into the native phase of another material (*e.g.*, dissolving $CO_2$ molecules into a liquid solution).[52] Membranes is another method that relies on the difference in solubility or diffusivity of $CO_2$ on both sides of the separation membrane to capture $CO_2$. As an energy-efficient method, membrane separation is considered to be the next generation of $CO_2$ separation technology. Due to the mechanism of the membrane process, the $CO_2$ content in mixed gas should be high enough to realize an efficient separation.[53] Since sorbents and solvents methods may have gas–liquid contact processes, they can be combined with the SLSO channel. Compared to packed towers and fluidized beds, which are involved in sorbents and solvents methods, this SLSO channel can achieve the ultimate reduction in overall volume while maintaining a large gas–liquid contact area. This facilitates the miniaturization of $CO_2$ capture devices.

As an ideal underwater gas carrier, further integration toward the applications in gas–liquid reactions should be designed and tested. We chose the absorption reaction of $CO_2$ and amine solution as a demonstration experiment. When the superhydrophobic channel and SLSO channel are immersed in 50% MDEA solution, the superhydrophobic channel will lose effectiveness in 12 h, while the SLSO channel will maintain the functions (Fig. S7, ESI†). These results indicate the potential for the SLSO hierarchical gas channel to be utilized as a submerged gas carrier in gas/liquid reactions under harsh environments. Based on the improved stability of this gas-manipulating interface, we designed the SLSO hierarchical gas channel as a gas/liquid exchanging microchip with continuous SLSO folded channels. As shown in Fig. 4(a), the upper side of the device is a

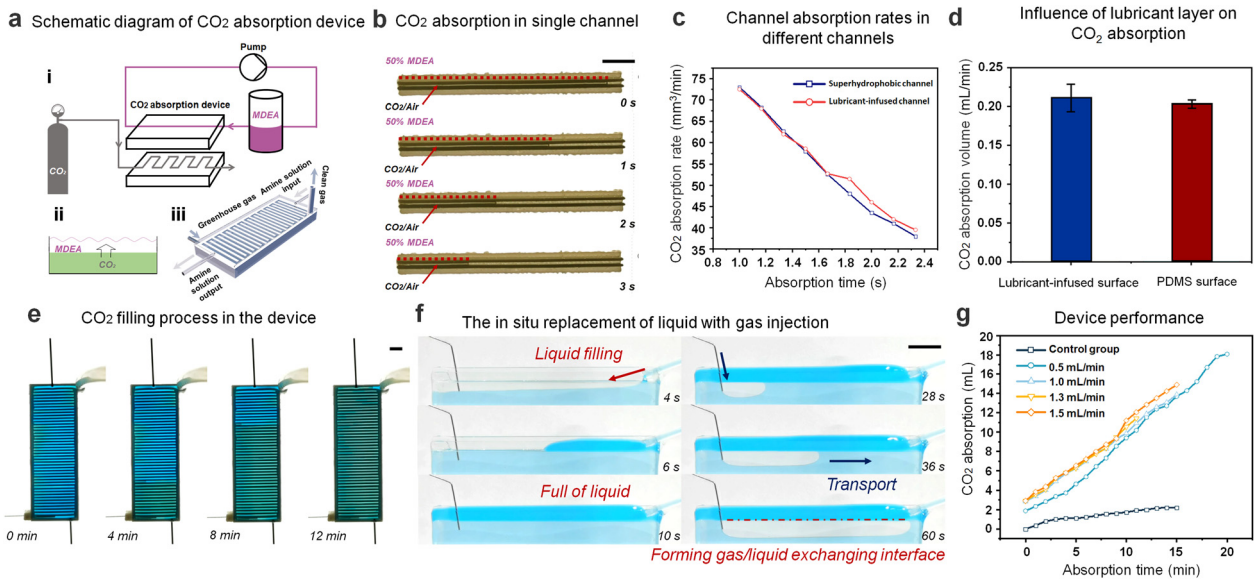


Fig. 4 $CO_2$ absorption with a SLSO channel-based microchip. (a) The process of on-chip $CO_2$ capture. The amine solution is circulated on the upper side and the $CO_2$/air mixture is continuously injected on the lower side (i), where the $CO_2$ is continuously absorbed by the amine solution at the gas–liquid interface (ii). (iii) Schematic diagram of the gas/liquid exchanging microchip with continuous SLSO folded channels. (b) The process of absorption of the $CO_2$/air mixture in a SLSO hierarchical gas channel immersed in 50% MDEA solution, scale bar = 1 cm. (c) The speed of reduction in the volume of the $CO_2$/air mixture column in the SLSO hierarchical channel and the superhydrophobic channel immersed in 50% MDEA solution, which can be shown without significant differences. (d) Absorption speed of $CO_2$ bubbles on the lubricant-infused surface and PDMS surface immersed in 50% MDEA solution. (e) The process of filling the $CO_2$ absorbing device with $CO_2$ gas. Scale bar 1 cm. (f) Demonstration of the process of injecting a bright blue stained amine solution in a single channel until it is full, then injecting $CO_2$ gas forward transport. The gas/liquid interaction process in the integrated $CO_2$ absorption device is similar to this. Scale bar = 1 cm. (g) The effect of $CO_2$ gas injection rate on the absorption rate of $CO_2$ absorption devices. The control group is the hollow microchip without a SLSO hierarchical channel. The result shows that the gas injection rate has little effect on the absorption rate of the devices due to the fast balance of $CO_2$ absorption. In contrast, the presence of channels has an obvious effect on the absorption rate of the devices, which indicates that the main factor affecting the absorption rate of $CO_2$ absorption devices is the gas/liquid contact area.

Published on 11 2023. Downloaded on 2024/10/12 2:17:48.

continuously circulating 50% MDEA solution, and the lower side is a continuously injecting $CO_2$/air mixture, which is continuously absorbed by the MDEA solution through staggered flow contact. Fig. 4(b) and Movie S12 (ESI†) show the $CO_2$ absorption process by placing a single channel SLSO hierarchical gas channel in 50% MDEA solution. In order to investigate whether the lubricant in the SLSO hierarchical gas channel affects the reaction rate of gas absorption, we compared the absorption rate of $CO_2$ gas columns in a single superhydrophobic channel and the SLSO hierarchical gas channel. No significant difference in the $CO_2$ absorption rate was observed between the two channels, as depicted in Fig. 4(c). Additionally, we also tested the absorption rate of $CO_2$ bubbles on the lubricant-infused surface and the PDMS surface, and found no significant difference in the absorption rate, as shown in Fig. 4(d) and Fig. S8 (ESI†). These results indicate that the lubricant-infused surface does not affect the rate of gas absorption. In conclusion, the lubricant-infused surface does not affect the rate of gas absorption. Overall, these findings demonstrate the potential of the SLSO hierarchical gas channel for use in gas/liquid reactions, and its compatibility with continuous operation strategies.

The process of injecting $CO_2$/air mixture into the gas/liquid exchanging microchip is depicted in Fig. 4(e) and Movie S13 (ESI†). To visualize the actual liquid and gas interaction process, a transparent single channel was utilized, as depicted in Fig. 4(f) and Movie S14 (ESI†). Initially, a bright blue-stained amine solution was injected above the channel, filling it entirely. Upon injection of the $CO_2$/air mixture, the gas spread forward along the channel, effectively replacing the liquid due to the stable gas capturing ability of the SLSO hierarchical gas channel. This reliable and continuous gas/liquid interaction allowed for easy $CO_2$ absorption by the MDEA solution in the channel. We compared the $CO_2$ absorption rates for different gas injection rates and found no significant difference. This observation can be mainly attributed to the fact that the MDEA solution is far from saturation during the $CO_2$ absorption process, allowing for consistent $CO_2$ absorption rates regardless of the gas injection rate. The $CO_2$ absorption rate was calculated by measuring the $CO_2$ absorption in the amine solution at different times of device operation. To determine the absorption rate for the $CO_2$ absorption device, an excess of hydrochloric acid solution was added to the amine solution to precipitate all $CO_2$. The amount of $CO_2$ absorption was then calculated using the volumetric method. Interestingly, we found that the absorption rate of $CO_2$ did not vary significantly for different gas injection rates due to the constant gas–liquid contact area (Fig. 4(d)). To corroborate these findings, we conducted a control experiment where the $CO_2$ absorption rate in a device of the same size without a gas channel was measured (Fig. S8, ESI†). The results showed that the absorption rate of gas was significantly lower, which could be attributed to the reduction of the gas–liquid contact area. Overall, the results suggest that the SLSO hierarchical gas channel has the potential to function effectively in gas/liquid exchanging processes such as $CO_2$ capture. The reliable performance of the SLSO microchannel system, in conjunction with continuous operation strategies, offers practical applications for gas absorption in various industries.

## Conclusions

The pitcher plant-inspired lubricant-infused surface is considered to be a stable surface for underwater gas manipulation. In this contribution, we reported a slippery/superaerophobic (SLSO) hierarchical gas channel with durable gas manipulation ability. The 3D printed open channel was treated as a hierarchical structure of an aerophilic lubricant-infused grooved channel and a superaerophobic edge for retaining gas. By varying the size and shape of the 3D printed channels, the underwater gas transferring process was regulated by different channels with U-shape, Y-shape, wave-shape, spiral and assembled structures. The SLSO hierarchical gas channel remains effective after 365 days of immersion in water, even when being treated at 2 atm or 20 kPa pressure for 2 h, *etc.* Finally, the SLSO hierarchical gas channel is designed as a gas/liquid exchanging microchip to achieve available $CO_2$ collection. The current design achieves an improved stability of underwater gas transporting interfaces, which should offer great opportunities to develop advanced systems relating to gas/liquid exchange and gas-involved reactions.

## Conflicts of interest

There are no conflicts to declare.

## Acknowledgements

This work was supported by the National Key R&D Program of China (2022YFA1504002), the National Natural Science Foundation of China (22075202, 21805204), the Haihe Laboratory of Sustainable Chemical Transformations, and Young Elite Scientists Sponsorship Program by Tianjin (TJSQNTJ-2018-17).

## Notes and references

1 W. Fang, C. T. Wang, Z. Q. Liu, L. Wang, L. Liu, H. J. Li, S. D. Xu, A. M. Zheng, X. D. Qin, L. J. Liu and F. S. Xiao, *Science*, 2022, **377**, 406–410.
2 L. Y. Li, Z. X. Li, W. J. Yang, Y. M. Huang, G. Huang, Q. Q. Guan, Y. M. Dong, J. L. Lu, S. H. Yu and H. L. Jiang, *Chem*, 2021, **7**, 686–698.
3 Y. X. Lv, X. H. Yu, J. J. Jia, S. T. Tu, J. Y. Yan and E. Dahlquist, *Appl. Energy*, 2012, **90**, 167–174.
4 Y. X. Sun, Q. Sun, H. L. Huang, B. Aguila, Z. Niu, J. A. Perman and S. Q. Ma, *J. Mater. Chem. A*, 2017, **5**, 18770–18776.
5 M. Paven, P. Papadopoulos, S. Schottler, X. Deng, V. Mailander, D. Vollmer and H. J. Butt, *Nat. Commun.*, 2013, **4**, 2512.
6 J. Luo, H. L. Yu, B. Y. Lu, D. H. Wang and X. Deng, *Small Methods*, 2022, **6**, 2201106.

 This journal is © The Royal Society of Chemistry 2023

Published on 11 2023. Downloaded on 2024/10/12 2:17:48.

7 Y. J. Lei, R. Z. Sun, X. C. Zhang, X. J. Feng and L. Jiang, *Adv. Mater.*, 2016, **28**, 1477–1481.
8 X. Sheng, Z. Liu, R. S. Zeng, L. P. Chen, X. J. Feng and L. Jiang, *J. Am. Chem. Soc.*, 2017, **139**, 12402–12405.
9 G. Jiang, L. Wang, Z. Tian, C. Chen, X. Hu, R. Peng, D. Li, H. Zhang, P. Fan and M. Zhong, *Mater. Horiz.*, 2023, DOI: 10.1039/D3MH00548H.
10 C. B. Wang, J. L. Wang, Z. T. Li, K. Y. Xu, T. Lei and W. K. Wang, *J. Mater. Chem. A*, 2020, **8**, 9528–9535.
11 B. Xu, A. Li, R. Wang, J. Zhang, Y. L. Ding, D. Pan and Z. J. Shen, *Adv. Funct. Mater.*, 2021, **31**, 2105265.
12 B. Dai, K. Li, L. X. Shi, X. Z. Wan, X. Liu, F. L. Zhang, L. Jiang and S. T. Wang, *Adv. Mater.*, 2019, **31**, 1904113.
13 Y. Y. Kong and J. H. Xin, *Adv. Eng. Mater.*, 2018, **20**, 1700905.
14 L. R. Shang, W. X. Zhang, K. Xu and Y. J. Zhao, *Mater. Horiz.*, 2019, **6**, 1080.
15 S. N. Zhang, J. Y. Huang, Z. Chen, S. Yang and Y. K. Lai, *J. Mater. Chem. A*, 2019, **7**, 38–63.
16 J. Xu, S. Xiu, Z. Lian, H. Yu and J. Cao, *Droplet*, 2022, **1**, 11–37.
17 H. Zhou, H. X. Wang, H. T. Niu and T. Lin, *Sci. Rep.*, 2013, **3**, 2964.
18 Y. F. Yang, H. Y. Bai, M. Q. Li, Z. Li, X. S. Wang, P. W. Wang and M. Y. Cao, *Mater. Horiz.*, 2022, **9**, 1888–1895.
19 K. H. Chu, R. Xiao and E. N. Wang, *Nat. Mater.*, 2010, **9**, 413–417.
20 S. L. Feng, P. A. Zhu, H. X. Zheng, H. Y. Zhan, C. Chen, J. Q. Li, L. Q. Wang, X. Yao, Y. H. Liu and Z. K. Wang, *Science*, 2021, **373**, 1344.
21 Y. X. Li, Z. H. Cui, G. Q. Li, H. Y. Bai, R. Y. Dai, Y. Z. Zhou, Y. Jiao, Y. G. Song, Y. Yang, S. Y. Liu and M. Y. Cao, *Adv. Funct. Mater.*, 2022, **32**, 2201035.
22 H. Y. Bai, X. S. Wang, Z. Li, H. Y. Wen, Y. F. Yang, M. Q. Li and M. Y. Cao, *Adv. Mater.*, 2023, **35**, 2211596.
23 M. S. Lehnert, D. Monaenkova, T. Andrukh, C. E. Beard, P. H. Adler and K. G. Kornev, *J. R. Soc., Interface*, 2013, **10**, 20130336.
24 P. Comanns, G. Buchberger, A. Buchsbaum, R. Baumgartner, A. Kogler, S. Bauer and W. Baumgartner, *J. R. Soc., Interface*, 2015, **12**, 20150415.
25 M. Prakash, D. Quere and J. W. M. Bush, *Science*, 2008, **320**, 931–934.
26 N. J. Shirtcliffe, G. McHale, M. I. Newton, C. C. Perry and F. B. Pyatt, *Appl. Phys. Lett.*, 2006, **89**, 104106.
27 X. Yan, W. Xu, Y. Deng, C. Zhang, H. Zheng, S. Yang, Y. Song, P. Li, X. Xu and Y. Hu, *Sci. Adv.*, 2022, **8**, eabo7698.
28 J. Sun, X. Qin, Y. Song, Z. Xu, C. Zhang, W. Wang, Z. Wang, B. Wang and Z. Wang, *Int. J. Extreme Manuf.*, 2023, **5**, 025504.
29 J. Xu, S. Xiu, Z. Lian, H. Yu and J. Cao, *Droplet*, 2022, **1**, 11–37.
30 H. C. Yang, J. W. Hou, L. S. Wan, V. Chen and Z. K. Xu, *Adv. Mater. Interfaces*, 2016, **3**, 1500774.
31 Y. C. Wu, J. G. Feng, H. F. Gao, X. J. Feng and L. Jiang, *Adv. Mater.*, 2019, **31**, 1800718.
32 Z. Y. Long, Y. Y. Zhao, C. H. Zhang, Y. H. Zhang, C. M. Yu, Y. C. Wu, J. Ma, M. Y. Cao and L. Jiang, *Adv. Mater.*, 2020, **32**, 1908099.
33 M. Dhar, U. I. Kara, S. Das, Y. Xu, S. Mandal, R. L. Dupont, E. C. Boerner, B. Y. Chen, Y. X. Yao, X. G. Wang and U. Manna, *Mater. Horiz.*, 2023, **10**, 2204–2214.
34 Y. A. Mehanna, E. Sadler, R. L. Upton, A. G. Kempchinsky, Y. Lu and C. R. Crick, *Chem. Soc. Rev.*, 2021, **50**, 6569–6612.
35 K. I. Hegner, W. S. Y. Wong and D. Vollmer, *Adv. Mater.*, 2021, **33**, 2101855.
36 C. Huang and Z. G. Guo, *Nanoscale*, 2018, **10**, 19659–19672.
37 X. Li, J. Zhang, X. Wang, D. Lv, C. Cao, L. Ai and X. Yao, *Droplet*, 2022, **1**, 65–75.
38 C. Lee and C. J. Kim, *Phys. Rev. Lett.*, 2011, **106**, 014502.
39 A. Martinez-Gomez, S. Lopez, T. Garcia, R. de Francisco, P. Tiemblo and N. Garcia, *ACS Omega*, 2017, **2**, 8928–8939.
40 J. S. Li, E. Ueda, D. Paulssen and P. A. Levkin, *Adv. Funct. Mater.*, 2019, **29**, 1802317.
41 T. S. Wong, S. H. Kang, S. K. Y. Tang, E. J. Smythe, B. D. Hatton, A. Grinthal and J. Aizenberg, *Nature*, 2011, **477**, 443–447.
42 X. S. Wang, H. Y. Bai, Z. Li and M. Y. Cao, *Soft Matter*, 2023, **19**, 588–608.
43 Y. L. Jiao, X. D. Lv, Y. Y. Zhang, C. Z. Li, J. W. Li, H. Wu, Y. Xiao, S. Z. Wu, Y. L. Hu, D. Wu and J. R. Chu, *Nanoscale*, 2019, **11**, 1370–1378.
44 C. M. Yu, X. B. Zhu, K. Li, M. Y. Cao and L. Jiang, *Adv. Funct. Mater.*, 2017, **27**, 1701605.
45 S. Kim, K. Han, W. Kim, S. Jeon and K. Yong, *Nano Energy*, 2019, **58**, 484–491.
46 A. Rico-Guevara and M. A. Rubega, *Proc. Natl. Acad. Sci. U. S. A.*, 2012, **109**, E867.
47 A. Rico-Guevara and M. A. Rubega, *Proc. Natl. Acad. Sci. U. S. A.*, 2011, **108**, 9356–9360.
48 P.-G. De Gennes, F. Brochard-Wyart and D. Quere, *Capillarity and Wetting Phenomena: Drops, Bubbles, Pearls, Waves*, Springer, 2004.
49 A. Keiser, P. Baumli, D. Vollmer and D. Quere, *Phys. Rev. Fluids*, 2020, **5**, 014005.
50 J. E. S. van der Hoeven, A. V. Shneidman, N. J. Nicolas and J. Aizenberg, *Acc. Chem. Res.*, 2022, **55**, 1809–1820.
51 X. S. Wang, H. Y. Bai, J. R. Yang, Z. Li, Y. C. Wu, C. M. Yu, L. Jiang and M. Y. Cao, *Small*, 2021, **17**, 2007803.
52 E. S. Sanz-Pérez, C. R. Murdock, S. A. Didas and C. W. Jones, *Chem. Rev.*, 2016, **116**, 11840–11876.
53 M. Rezakazemi, A. E. Amooghin, M. M. Montazer-Rahmati, A. F. Ismail and T. Matsuura, *Prog. Polym. Sci.*, 2014, **39**, 817–861.